Design of Dynamically Balanced Gait for the Biped Robot While Crossing the Ditch

Moh Shahid Khan*, Ravi Kumar Mandava

Mechanical Engineering Department, Maulana Azad National Institute of Technology, Bhopal, Madhya Pradesh, India 462003;
E-mail: 203116026@stu.manit.ac.in; ravikumar1013@manit.ac.in
*Corresponding author

Abstract: The current research work aims to generate the dynamically balanced gait for the 16-DOF biped robot while crossing the ditch by using the concept of the zero moment point (ZMP). Initially, forward kinematics was established to obtain the position and orientation of the biped robot while crossing the ditch. The various joint angles of the biped robot were estimated by deriving the inverse kinematics. Further, the dynamics of the biped robot was obtained using the Lagrange-Euler formulation. A cubic polynomial equation was assigned for the smooth motion of foot and wrist trajectories in the sagittal plane and hip trajectory in the horizontal plane. The obtained cubic polynomial trajectory for the foot was compared with the second-order and fifth-order polynomial trajectories in terms of dynamic balance margin (DBM). A simulation study was conducted to verify the dynamically balanced gait while crossing the ditch. Finally, the generated gait angles were tested on a real 16-DOF biped robot. It has been found that the generated gait is more dynamically balanced while crossing the ditch.

Keywords: Biped robot; gait generation; ditch crossing; DBM; ZMP; Lagrange-Euler formulation

1 Introduction

Bipedal robots have many advantages over other wheeled robots due to their similar characteristics to human beings. That similarity creates complexity for building a biped robot and enabling it to perform human actions due to the very complex and multi-degrees of freedom (DOF) mechanism. The most crucial and significant requirement for developing biped robots is the ability to move across various terrains. Around the world, many researchers are working on the dynamically balanced gait generation of the biped robot on various uneven terrains. The gait cycle consists of two phases that is, the single support phase (SSP) and the double support phase (DSP). The dynamic stability of the biped robot during the gait cycle can be obtained from the concept of the zero moment point (ZMP) [1]. Chow and Jacobson [2] applied the Lyapunov function, the linear feedback principle, and an

on-off perturbation to generate the gait on a flat surface. Townsend and Tsai [3] generated a variety of gaits on both SSP and DSP by using various initial parameters. In addition, Katoh and Mori [4], [5] presented a control method for a 4-DOF biped robot by using Van Der Pol's equation and obtained stable limit cycles. Mita et al. [6] generated the Chiba Walker 1 (CW-1) mechanism, which requires one second to complete each step with a step length of less than 20 cm. Further, Hürmüzlü and Moskowitz [7] developed a mathematical model based on LIPM (linear inverted pendulum model) to address the impact of periodic force on the stability of biped locomotion. Takanishi et al. [8] stabilized the gait patterns while walking under the influence of a known external unbalanced force produced by a DD (direct drive) motor for the WL-12R biped robot. Then, the researchers proposed a control method that recognizes the geometry of the terrain, which allowed the biped robot WL-12RIII to walk on stairs with a 0.1-meter step height and $\pm 10^{\circ}$ inclined trapezoidal terrain [9]. Moreover, Zheng [10] discussed an autonomous gait generation for biped robots to walk on complex terrains with the help of a central pattern generator (CPG) and the concept of neural network (NN). Later on, Thomas Miller [11] proposed a hierarchical control for a 10-axis biped model using a PID controller and a cerebellar model arithmetic computer (CMAC) NN learning system. Also, Arakawa and Fukuda [12] established an ideal gait for a 13-DOF biped robot by reducing energy consumption by using the concept of ZMP and genetic algorithm (GA). To generate the stable gait for the 6-link biped robot, Magdalena and Monasterio-Huelin [13] developed a learning mechanism by using GA and a fuzzy logic controller (FLC). GA helps to modify the fuzzy rules and their functions relevant to the human information database. Abba & Chaillet [14], established bidirectional dynamic modelling by using the features of the epicyclic gear train, and computed torque control (CTC). In [15], the authors used a V-HRP (Virtual Humanoid Robot Platform) simulator to verify the robot simulation virtually before going to test in a real-time environment. The said robot consists of 26-DOF and a height of 540 mm equipped with a CCD camera, foot sensors, a posture sensor, and a USB. Chestnutt et al. [16] proposed an architecture for an H7 humanoid robot to walk on uneven ground along with obstacles. In addition, Sabourin and Bruneau [17] discussed a CMAC-NN-based control strategy for fast walking of a virtual under-actuated biped robot. After learning, the NN first generates the passive and active gaits of the biped robot. Puga et al. [18] obtained a distributed control scheme that consists of a fractional-order PID controller optimized by a GA. The control parameters were tested on a 22-DOF small-sized humanoid robot. Further, Ghorbani et al. [19] developed a control scheme using a general regression NN (GRNN) feedback control and a PID feedback controller with Lyapunov exponents to stabilize the LIPB-based biped model. A Genetic algorithm is used to optimize the GRNN controller to reduce energy consumption and create a closed-loop learning controller.

Vundavilli and Pratihar [20] suggested an analytical method for a 7-DOF biped robot with the help of the inverse dynamics trained neural network (NN) to generate the gait on staircases, sloping surfaces, and ditches. Further in [21], [22], they

discussed the optimal online gait generation of the biped robot using NN and FL-based gait planners which was trained by GA. In addition, Fattah and Fakhari [23] established a trajectory planning algorithm for a seven-link planar biped robot with variable step lengths on level ground along with ditches. Sudheer et al. [24] suggested a framework for an eight-link biped robot to solve the kinematics and dynamics based on the ZMP constraint and optimized using a simulated annealing approach. A cycloidal trajectory was assigned for the swing foot and the modified Cartesian cycloid trajectory for the hip. Kalamian and Farrokhi [25] proposed a nonlinear model predictive control (NMPC) algorithm to generate the gait while crossing the obstacle at a speed of 1 m/s. Moreover, Lathan et al. [26] suggested an analytical method of a 7-DOF biped robot to generate a dynamically balanced gait while crossing and stepping over the obstacle. R. Kumar et al. [27] developed the neural network (NN) based gait planners for a biped robot for crossing obstacles. The weights of the NN algorithm were optimized by GA and differential evolution (DE) algorithms. Later, Mandava and Vundavilli [28]–[30] developed a framework for generating whole-body motions of an 18-DOF humanoid robot using the concept of inverse kinematics. Bai et al. [31] discussed a dynamically balanced gait generation of the humanoid robot while crossing over obstacles with the help of a pulsing type joint. The said humanoid robot is capable of squatting and displacing heavy objects from one place to another. Furthermore, Anh and Huan [32] established a method for optimizing the gait generation of a 10-DOF biped robot. The modified Jaya algorithm was used to optimize the distance between the ZMP and the foot center then said approach was tested on HUBOT-4. Also, Tsuru et al. [33] proposed a structure of an autonomous humanoid robot for finding and holding objects in unknown surroundings. The proposed methodology was experimentally applied to HRP2-KAI and validated its efficiency. Yang et al. [34] discussed an NN estimator with an incremental learning mechanism while obtaining a new online walking controller for biped robots. The proposed method controls the ZMP stability while compensating for the yaw moment. Later on, researchers developed various methodologies to generate the gait for avoiding obstacles, stepping over them, and crossing ditches. Kashyap et al. [35] developed an Improved Modified Chaotic Invasive Weed Optimization (IMCIWO) algorithm to navigate the humanoid robot and avoid obstacles. The authors conducted a simulation on the NAO humanoid robot in WEBOT software. In [36], established a model predictive controller (MPC) for NAO humanoid robot while walking on uneven terrain, in an unknown environment and stepping over obstacles. Janardhan and Kumar [37] proposed a multibody dynamics framework for gait generation of the 5-DOF biped robot while crossing the ditches. The width of the ditch is greater than the length of the leg. Gupta and Dutta [38] developed a trajectory and navigation planner for a 12-DOF biped robot while walking on uneven terrain along with obstacles.

Apart from the above discussion, some researchers have developed various techniques for generating a dynamically balanced gait for the biped robot as it crosses the ditch. To generate the systematic gait a cubic polynomial trajectory was assigned for the foot in the sagittal plane and the hip in the horizontal plane.

In addition, an inverse kinematics approach is established for obtaining the various joint angles of the biped robot along with foot trajectory. Moreover, the balancing of the biped robot is calculated using the concept of ZMP and measured in terms of DBM. Further, the dynamics of the biped robot is obtained by using the Lagrange-Euler formulation which is useful to determine the torque required for each joint of the robot. Additionally, it has been noted that only a few researchers have developed real-time biped robots for verifying the gait while crossing a ditch. In the present research work, the authors have developed a real biped robot titled AZAD-16, which consists of 16-DOF for verifying the simulations in a real-time environment.

The rest of the article is organized as follows: Section 2 explains the mathematical modelling of the biped robot, which includes the physical dimensions of AZAD-16, trajectory generation for the foot, hip, and arm, forward and inverse kinematics, DBM as fundamental stability criteria, and the Lagrange-Euler (LE) algorithm for estimating the dynamics. Further, the results and discussions of the current research work are discussed in Section 3. Finally, Section 4 provides the conclusions of the proposed research work.

2 Mathematical Modelling

AZAD-16 is a tiny biped robot that was built in our laboratory which is shown in Figure 1(a). The trunk and various brackets for holding the servo motors were made by 3D printing. All the joints of the 16-DOF biped robot consist of rotatory joints which are shown in Figure 1(b). The weight and height of the robot is 5 kg and 480 mm. Each leg of the biped robot consists of 5-DOF mobility which contributes 2-DOF for hip joint, 2-DOF for the ankle joint and 1-DOF for the knee joint. However, each arm has 3-DOF mobility, which contributes 2-DOF for the shoulder and 1-DOF for the elbow joint. The joints of the legs are attached with 60 kg-cm rated servo motors and the joints of the arms are attached with 35 kg-cm rated servo motors. Various input parameters such as power rating, type of actuation, link length and mass related to the AZAD-16 biped robot are shown in Table 1.

Table 1
Various input parameters of the "AZAD-16"

AZAD-16	Joints Name	Power Rating (Kg-cm)	Type of Actuation	Link's Name	Link Length (mm)	Link Mass (Kg)
Right Leg	Hip	60	Yaw	-	35.12	0.15
		60	Pitch	Thigh	93.87	0.25
	Knee	60	Pitch	Shank	67.00	0.25
	Ankle	60	Pitch	-	35.24	0.15
		60	Yaw	-	42.50	0.15

Left Leg	Hip	60	Yaw	-	35.12	0.15
		60	Pitch	Thigh	93.87	0.25
	Knee	60	Pitch	Shank	67.00	0.25
	Ankle	60	Pitch	-	35.24	0.15
		60	Yaw	-	42.50	0.15
Right Arm	Shoulder	60	Pitch	-	33.00	0.25
		35	Yaw	Arm	93.76	0.1
	Elbow	35	Pitch	Forearm	93.76	0.1
Left Arm	Shoulder	60	Pitch	-	33.00	0.25
		35	Yaw	Arm	93.76	0.1
	Elbow	35	Pitch	Forearm	93.76	0.1
Trunk	-	-	-	Height	175.00	0.3
				Front Width	165.00	
				Side Width	70.00	

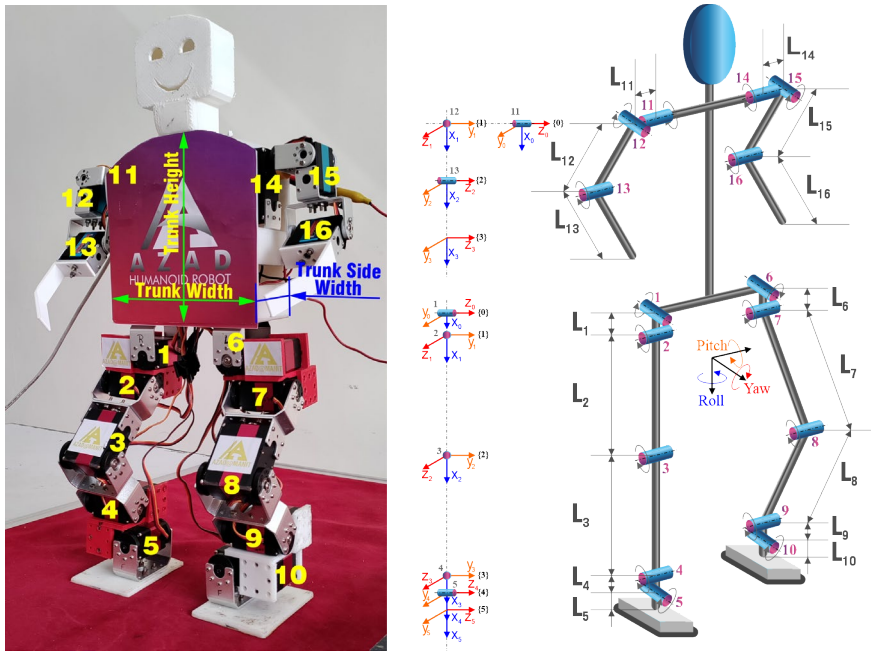

(a) (b)

Figure 1
Schematic diagram showing the (a) real biped robot that is AZAD-16 and (b) kinematic model displaying the positioning and coordinate frames for various joints

2.1 Trajectory Generation for Foot, Hip, and Arm

The foot, hip, and arm of the robot AZAD-16 follow a polynomial trajectory while crossing the ditch. The terms z and x have been considered the height and length of the polynomial at a particular time interval. Where, $\mu_0, \mu_1, \mu_2 \ldots \ldots \mu_n$ have been taken as coefficients of the polynomial equation, respectively. The initial and final positions of the foot have been considered x_1, x_2 and x_3. In the present research problem, the foot trajectory of the robot is considered quadratic, cubic and fifth ordered polynomial equations and compared the results in terms of dynamic balance margin. Further, hip trajectory in horizontal plane and wrist trajectory in sagittal plane have been assigned as cubic polynomial trajectory. The distances between the trunk and wrist end at initial and final instances of wrist trajectory are x_{01} and x_{03}, respectively. The height of the hip joint and width of the ditch are represented as H and d_w. The boundary conditions for generating various polynomial trajectories for the foot, hip and wrist are shown in Table 2.

Table 2
Boundary conditions for different trajectories of wrist, hip and swing foot in various planes

▪ **Wrist Trajectory (Sagittal View)**	
Cubic Polynomial, $z = \mu_0 + \mu_1 x + \mu_2 x^2 + \mu_3 x^3$	
x	**z**
x_{01}	h
$x_{01} + (d_w/2)$	$h + (d_w/8)$
$x_{01} + (3d_w/2)$	$h + (d_w/8)$
x_{03}	h

▪ **Hip Trajectory (Top View / Horizontal Plane)**	
Cubic Polynomial, $z = \mu_0 + \mu_1 x + \mu_2 x^2 + \mu_3 x^3$	
x	**z**
x_1	0
$x_1 + (d_w/2)$	$d_w/10$
$x_1 + (3d_w/2)$	$d_w/10$
x_3	0

▪ **Swing Foot Trajectory (Sagittal View)**					
Quadratic		**Cubic Polynomial**		**Fifth Order Polynomial**	
$z = \mu_1 x + \mu_2 x^2$		$z = \mu_0 + \mu_1 x + \mu_2 x^2 + \mu_3 x^3$		$z = \mu_0 + \mu_1 x + \mu_2 x^2 + \mu_3 x^3 + \mu_4 x^4 + \mu_5 x^5$	
x	**z**	**x**	**z**	**x**	**z**
x_1	0	x_1	0	x_1	0
$x_3 - (x_1/2)$	$d_w/2$	$x_1 + (d_w/2)$	$d_w/3$	$x_1 + (2d_w/5)$	$d_w/4$
x_3	0	$x_1 + (3d_w/2)$	$d_w/3$	$x_1 + (4d_w/5)$	$d_w/2$
		x_3	0	$x_1 + (6d_w/5)$	$d_w/2$
				$x_1 + (8d_w/5)$	$d_w/4$
				x_3	0

2.2 Forward & Inverse Kinematics of the Biped Robot

The main aim of this research is to generate a 3D smooth gait while crossing the ditch in both sagittal and frontal planes. Figure 2 shows the schematic diagram of the biped robot while crossing the ditch in both sagittal and frontal planes, respectively. To generate the gait cycle systematically a forward kinematic analysis is essential. Initially, the coordinate frames are assigned at each joint of the biped robot and Denavit-Hartenberg (D-H) notation is used for obtaining the position and orientation of the end effector. Table 2 shows the D-H parameters for two legs and two hands of AZAD-16.

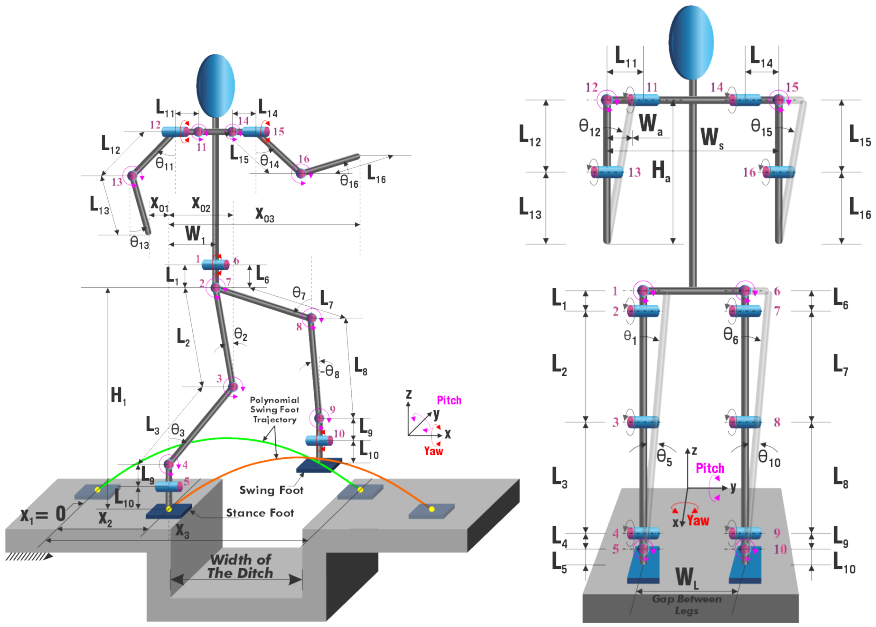

(a) (b)

Figure 2
Schematic model of AZAD-16 demonstrating the various revolute joint angles in the (a) sagittal plane and (b) frontal plane

Table 3
DH parameters of AZAD-16

Frames	Link	Joint Angle (θ_i)	Twist Angle (α_i)	Link Length (a_i)	Joint Offset (b_i)
•	**Right Leg**				
0 to 1	1	θ_1	90	L_1	0
1 to 2	2	θ_2	0	L_2	0
2 to 3	3	θ_3	0	L_3	0
3 to 4	4	θ_4	-90	L_4	0
4 to 5	5	θ_5	0	L_5	0

•	**Left Leg**				
0 to 1	6	θ_6	90	L_6	0
1 to 2	7	θ_7	0	L_7	0
2 to 3	8	θ_8	0	L_8	0
3 to 4	9	θ_9	-90	L_9	0
4 to 5	10	θ_{10}	0	L_{10}	0
•	**Right Arm**				
0 to 1	11	θ_{11}	90	L_{11}	Y_1
1 to 2	12	θ_{12}	-90	L_{12}	0
2 to 3	13	θ_{13}	0	L_{13}	0
•	**Left Arm**				
0 to 1	14	θ_{14}	90	L_{14}	Y_1
1 to 2	15	θ_{15}	-90	L_{15}	0
2 to 3	16	θ_{16}	0	L_{16}	0

Once the polynomial trajectories are assigned for the foot and wrist in the sagittal plane and the hip in the horizontal plane, the gait generated from the various limbs of the biped robot is calculated from the concept of inverse kinematics. The initial joint angles of the upper and lower limbs of the swing leg (that is, θ_2 and θ_3) are obtained by using a closed form of inverse kinematic equations given in Eqn. (1) and Eqn. (2).

$$\theta_3 = sin^{-1}\left(\frac{H_1 L_2 \sin\vartheta + W_1(L_3 + L_2 cos\vartheta)}{(L_3 + L_2 cos\vartheta)^2 + (L_2 sin\vartheta)^2}\right) \tag{1}$$

$$\vartheta = cos^{-1}\left(\frac{{H_1}^2 + {W_1}^2 - {L_2}^2 - {L_3}^2}{2L_2L_3}\right) \tag{2}$$

Where H_1 is the height of the hip from the swing foot which can be calculated by using the relation $H_1 = L_3 cos\theta_3 + L_2 cos\theta_2$; and W_1 is the distance measured from the swing foot to the hip in 'X' direction which can be calculated from the following relation that is, $W_1 = L_3 sin\theta_3 + L_2 sin\theta_2$; Further, the joint angle θ_2 obtained from the following relation that is, $\theta_2 = \theta_3 - \vartheta$.

Similarly, the joint angles (that is, θ_{11} and θ_{13}) of the swing hand in sagittal plane is obtained by following Eqn. (3) and Eqn. (4).

$$\theta_{11} = cos^{-1}\left(\frac{{H_h}^2 + {W_h}^2 + {L_{12}}^2 - {L_{13}}^2}{2L_{12}\sqrt{{H_h}^2 + {W_h}^2}}\right) + \beta \tag{3}$$

$$\theta_{13} = sin^{-1}\left(W_h - \left(L_{12} sin\left(\frac{\theta_{11}}{\theta_{13}}\right)\right)\right) \tag{4}$$

Where H_h is height of the hand in wrist position to shoulder ($H_h = L_{12} cos\theta_{11} + L_{13} cos\theta_{13}$); and W_h is width of the hand in wrist to trunk ($W_h = L_{12} sin\theta_{11} + L_{13} sin\theta_{13}$). Moreover, the value β is calculated by using the following relation (that is, $\beta = tan^{-1}\left(\frac{W_h}{H_h}\right)$.

Further, the various joint angles (that is, $\theta_1, \theta_5, \theta_6, \theta_{10}, \theta_{12}, and\ \theta_{15}$) of the biped robot in frontal plane are given below.

$$\theta_1 = \theta_6 = tan^{-1}\left(\frac{W_L}{H_1}\right) \tag{5}$$

$$\theta_5 = \theta_{10} = tan^{-1}\left(\frac{W_L}{2H_2}\right) \tag{6}$$

$$\theta_{12} = \theta_{15} = tan^{-1}\left(\frac{W_a}{H_a}\right) \tag{7}$$

Where $H_2 = L_7 cos\theta_7 + L_8 cos\theta_8$, height of the arm $H_a = L_{15} cos\theta_{14} + L_{16} cos\theta_{16}$, $W_a = W_s/8$, W_s is distance between shoulder joints, and W_L is the distance between both legs.

2.3 Dynamic Balance Margin

In the current study, the stability of the biped robot while crossing the ditch is obtained by the concept of ZMP. The ZMP in the x and y directions is calculated by using the following Eqn. (8) and Eqn. (9), respectively.

$$x_{ZMP} = \frac{\sum_{i=1}^{16}(-I_i\dot{\omega}_i + m_i x_i(\ddot{z}_i - g) + m_i\ddot{x}_i z_i)}{\sum_{i=1}^{16} m_i(\ddot{z}_i - g)} \tag{8}$$

$$y_{ZMP} = \frac{\sum_{i=1}^{16}(-I_i\dot{\omega}_i + m_i y_i(\ddot{z}_i - g) + m_i\ddot{y}_i z_i)}{\sum_{i=1}^{16} m_i(\ddot{z}_i - g)} \tag{9}$$

Where x_i, y_i, and z_i indicate the lumped mass coordinates, I_i represent the moment of inertia of the link in (kg-m^2), $\dot{\omega}_i$ denotes angular acceleration in (rad/s^2), m_i represents the mass of the link (kg), g indicates the acceleration due to gravity (m/s^2), and $\ddot{x}_i, \ddot{y}_i, and\ \ddot{z}_i$ represent acceleration in x, y and z direction for i^{th} link in (m/s^2).

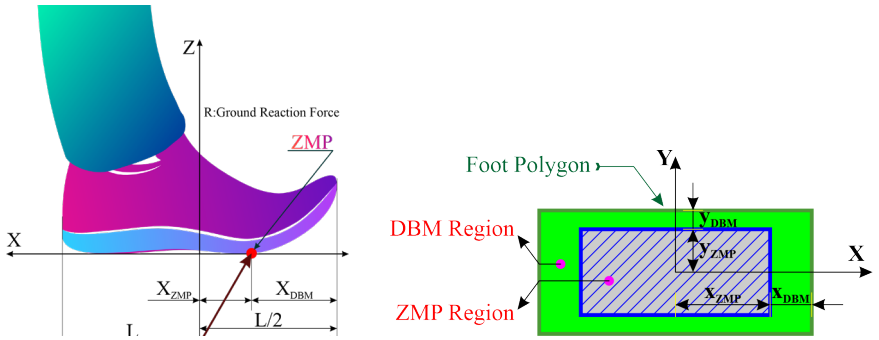

(a) (b)

Figure 3
Schematic diagram showing (a) relation between ZMP and DBM, (b) top view of foot support showing ZMP region enclosed under DBM region

If the ZMP is falling nearer to the center of the foot, then the robot is more dynamically balanced. Suppose the ZMP does not fall inside the foot support polygon then move all the links and joints of the biped robot systematically towards the center of the foot. Therefore, the ZMP pushes inside the foot support polygon. Figure 3 shows the regions of ZMP and DBM in x and y directions along with ZMP. The DBM of the biped robot is calculated by following relations.

$$x_{DBM} = \frac{Length\ of\ the\ foot\ support}{2} - |x_{ZMP}| \tag{10}$$

$$y_{DBM} = \frac{Width\ of\ the\ foot\ support}{2} - |y_{ZMP}| \tag{11}$$

2.4 Dynamic Analysis of the Biped Robot

The dynamics of the 16-DOF biped robot is useful to estimate the torque required at each joint. In the current research work, the authors have considered the Lagrange Euler (L-E) formulation for calculating the dynamics. The torque required (τ_i) at each joint is calculated by the following equations.

$$\tau_i = \sum_{j=1}^{n} M_{ij}(\theta)\ddot{\theta}_j + \sum_{j=1}^{n}\sum_{k=1}^{n} h_{ijk}\dot{\theta}_j\dot{\theta}_k + G_i \tag{12}$$

Where $i, j = 1, 2, 3 \ldots\ldots\ldots\ldots 16;$ $\theta, \dot{\theta}_j\ and\ \ddot{\theta}_j$ are represented as angular displacement, angular velocity and angular acceleration at various joints. Further, the expanded terms of inertia forces (M_{ij}), centrifugal/Coriolis forces (h_{ijk}) and gravity forces (G_i) are provided below.

Inertia term, $M_{ij} = \sum_{p=\max(i,j)}^{n} Trace\left[d_{pj} I_p d_{pi}^T\right]$ (13)

Centrifugal/ Coriolis acceleration term,

$$h_{ijk} = \sum_{p=\max(i,j)}^{n} Trace\left[\frac{\partial(d_{pj})}{\partial\theta_k} I_p d_{pi}^T\right] \tag{14}$$

Gravity term, $G_i = -\sum_{p=i}^{n} m_p g d_{pi}\, {}^{p}\bar{r}_p$ (15)

Where I_p, ${}^{p}\bar{r}_p$ and g indicate the moment of inertia (kg-m/sec^2), the center of mass location (m) and acceleration due to gravity (m/ sec^2), respectively.

The amount of average power required for a 16-DOF biped robot to generate the gait while crossing the ditch is determined by the estimated torque and angular velocity of each joint. The equation required for calculating the average power is as follows.

Power Consumption, $P = \sum_{i=1}^{16} \int_{t_0}^{t_f} \left|\tau_i(t)\dot{\theta}_i(t)\right| dt$ (16)

Here, t_0 and t_f represent the initial and final times, respectively. To achieve the desired angular displacement, it is necessary to determine the precise amount of joint acceleration that needs to be delivered to the actuator. The equation for joint acceleration ($\ddot{\theta}$) can be obtained by solving Eqn. 12, which is shown in Eqn. 17.

$$\ddot{\theta}_j = \tau_{i,actual} + \sum_{j=1}^{n} M_{ij}(\theta)^{-1}\left[-G_i - \sum_{j=1}^{n}\sum_{k=1}^{n} h_{ijk}\dot{\theta}_j\dot{\theta}_k\right] \quad (17)$$

Where $\tau_{i,actual} = \tau_i \sum_{j=1}^{n} M_{ij}(\theta)^{-1}$, represents the actual amount of torque required at each individual joint or servo actuator to rotate it by $\theta_{i,final} - \theta_{i,initial}$.

3 Results and Discussions

Once the mathematical model is developed the performance of the biped robot is measured in terms of dynamic balance margin while crossing the ditch in terms of computer simulations as well as the real biped robot that is, AZAD-16. The designed gait generation algorithm requires the initial position of the upper and lower links of the swing leg and hand. The necessary joint angles of the swing leg are $\theta_2 = 40^{\circ}$, and $\theta_3 = -30^{\circ}$; similarly, the initial joint angles of the; swing hand are $\theta_{10} = 40^{\circ}$ and $\theta_{13} = -40^{\circ}$ respectively. Initially, the DBM of the biped robot is tested in terms of swing foot trajectory. In this research, the authors assigned three varieties of swing foot trajectories which are derived from quintic, cubic and quadratic polynomial equations as shown in Figure 4 (a). The initial boundary condition of the swing foot was taken as, $x_1 = 0$ over a step length of 0.1382 m. The horizontal distance, or step size and time restriction for the gait cycle are constant for all situations. The wrist trajectory of both hands which were obtained from the cubic polynomial equations in the sagittal plane as shown in Figure 4 (b). Furthermore, Figures 4 (c) and 4 (d) depict the hip trajectory of the biped robot in the top or horizontal plane and sagittal plane which were derived as cubic polynomial and straight-line trajectories respectively. It is to be noted that the execution of the generated ditch crossing gait results in a straight-line horizontal hip trajectory or constant hip height throughout the gait which helps to maintain the dynamic balancing of the biped robot while performing the gait.

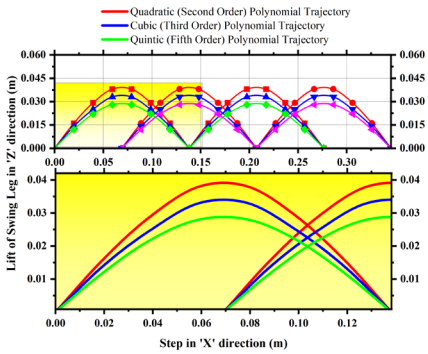

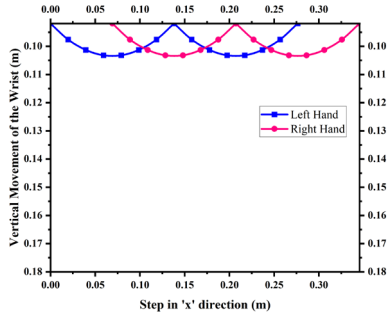

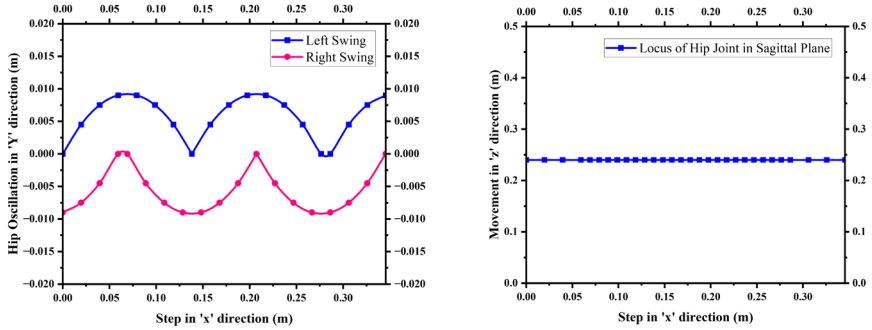

Figure 4

Graph showing (a) various foot trajectories in sagittal plane, (b) cubic polynomial trajectory of wrist end in sagittal plane, (c) cubic polynomial hip trajectory in top plane and (d) straight line hip trajectory in sagittal plane representing locus of hip height along 'x' direction

The results related to the swing foot trajectory are compared with the quadratic (second order) and quintic (fifth order) polynomial swing foot trajectories in terms of ZMP and DBM. Figures 5 (a) and (b) illustrate the variation of the ZMP measurement for all swing foot trajectories in the X and Y directions where the center of the stance foot is indicated by the zero value of the vertical axis. Further, Figures 6 (a) and (b) show the variation of DBM in X and Y direction. The investigation reveals that the cubic polynomial swing foot trajectory performs more dynamically balanced gaits when compared with quadratic and quintic polynomials. Because the ZMP is falling closer to the center of the foot in the case of cubic polynomial swing foot trajectory when compared with the quadratic and quintic polynomial trajectory. In addition, Figures 7 (a) and (b) depict the average DBM of the biped robot while crossing the ditch after assigning the quadratic, cubic and quintic polynomial trajectories in both X and Y directions. It has been observed that the cubic polynomial swing foot trajectory is more dynamically balanced when compared to quadratic and quintic polynomial trajectories.

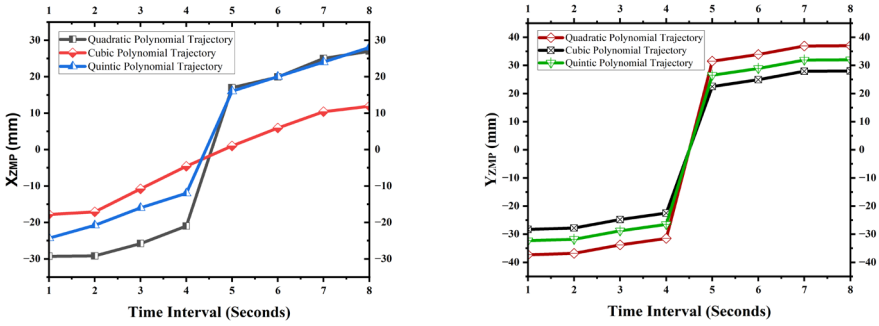

Figure 5

Variation of ZMP (a) X-direction and (b) Y- direction

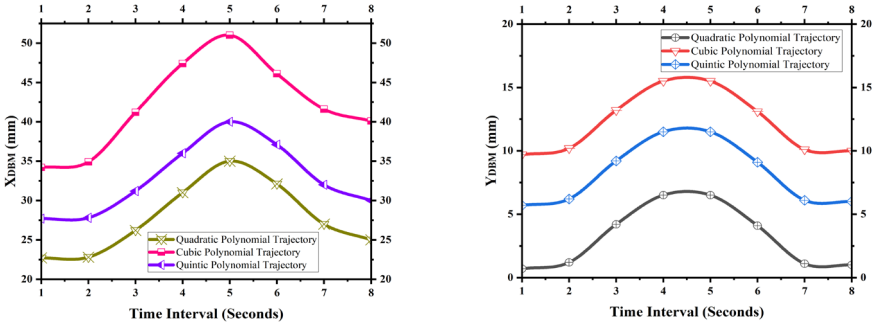

Figure 6
Variation of DBM (a) X-direction and (b) Y- direction

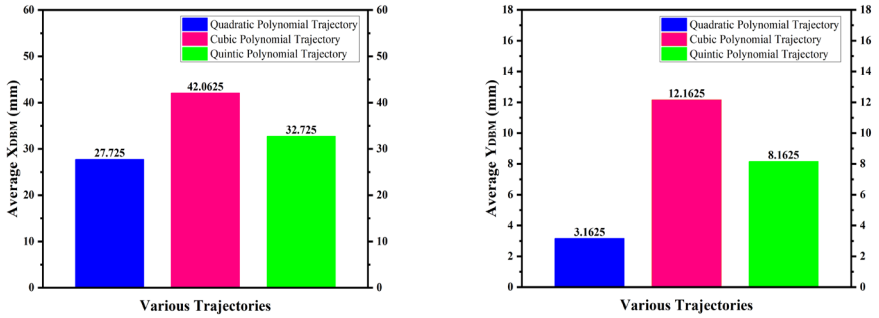

Figure 7
The bar chart shows the average DBM (a) in the x direction and (b) in the y direction as a consequence of various polynomial trajectories of the swing foot

Figure 8 (a) shows the variation of joint angles obtained from various joints of the biped robot only for the case of cubic polynomial swing foot trajectory while crossing the ditch in both SSP and DSP. The variation in the joint angles θ_2, θ_3, θ_4, θ_7, θ_8, θ_9, θ_{11}, θ_{13}, and θ_{16} causes the pitch motion of servo actuators and variation in the joint angles θ_1, θ_5, θ_6, θ_{10}, θ_{12}, and θ_{15} causes yaw motion in servo actuators for both SSP and DSP cases. It has been observed that the variation of joint angles in SSP is high. Whereas in DSP, the variation of joint angles is very less due to short time intervals of time. It has also been observed that the hip joints 2 and 6 are producing the pitch motion that is necessary to generate the ditch crossing gait and is showing a huge variation as depicted in Figure 8 (a), the joints 3–8, 4–9, 11–14, and 13–16 are obtaining the similar trend. Similarly, Figure 8 (b) shows the variation of angular velocity for all joints of the biped robot while crossing the ditch. It has been observed that the corresponding revolute joints 11 and 14 demonstrate a significantly higher variation in the angular velocity (rad/s) followed by joints 13 and 16 in DSP. DSP phases. The angular velocity changes from positive to negative which indicates the acceleration and deceleration within the gait range during the DSP phase.

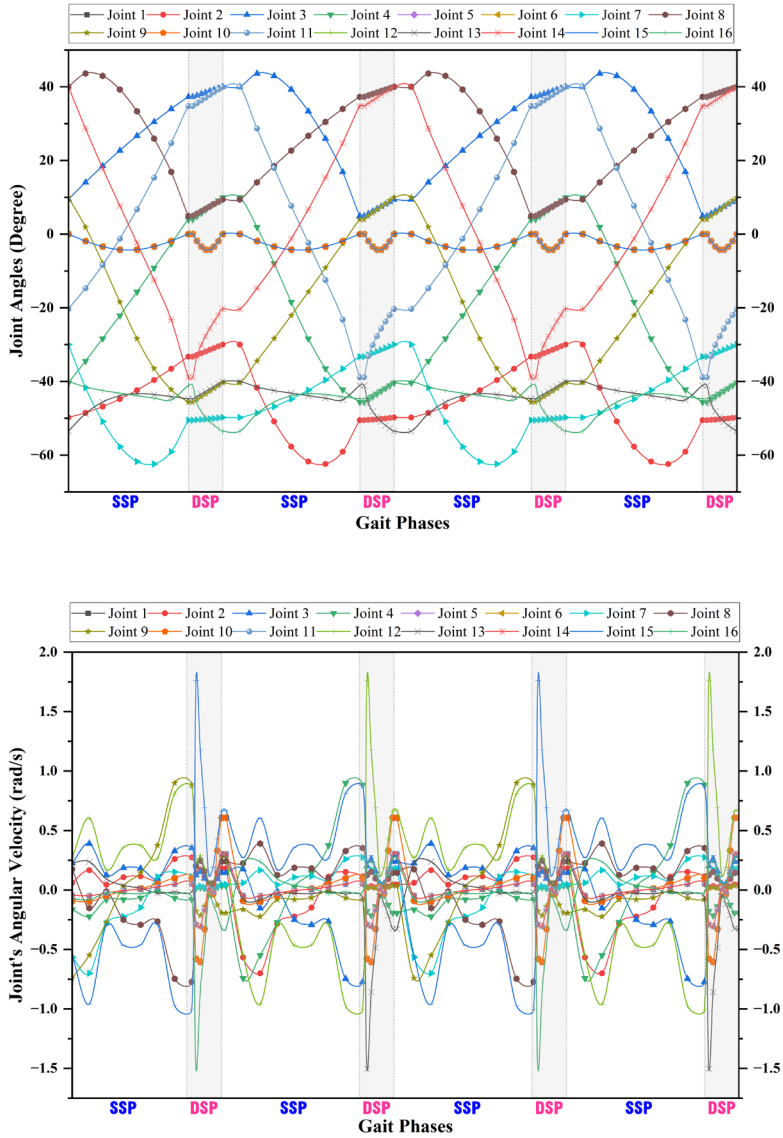

Figure 8

Variation of the joint parameters in SSP compared with its variation in DSP. (a) joint angles and (b) joint angular velocity

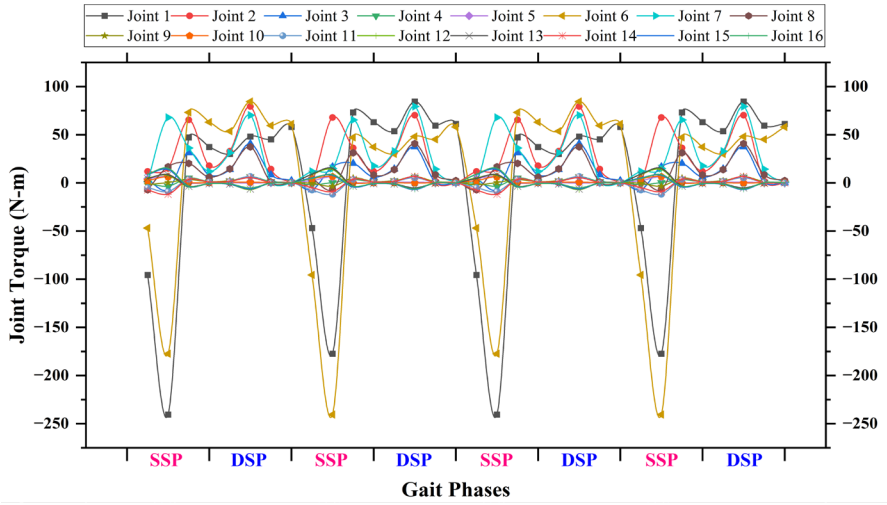

Schematic diagram showing the variation of torque required at various joints of the biped robot.

The cyclic variations in the magnitude of the actuator torque produced at each joint of the biped robot at various gait phases are shown in Figure 9. From Figure 9, it can be seen that the torque required at the hip joint is more than other joints. The magnitude of required joint torque is highest for yaw (joints 1 and 6) and pitch (joints 2 and 7) motions for both swing and stance legs. Because while exchanging the leg support, the hip joint of the leg carries the weight of the lower links and joints of the swing leg. It has been found that the hip joint of the stance leg consumes more torque when compared to the hip joint of the swing leg. Because the hip joint of the stance leg supports the whole body without falling on the ground. Further, figure 10 shows the average power consumption at various joints of the biped robot while crossing the ditch. It is important to note that, the power consumption is the product of individual joint torque and angular velocity. Despite, the highest torque obtained at joints 1 and 6, it has been observed that the power consumption is comparatively smaller than joint 7 due to lower angular velocity and the least variation of the joint angles throughout the gait cycle. Whereas joint 7 experiences the higher variation of joint angles and consequently consumes the highest power individually.

Figure 11 shows the simulation results of the 16-DOF biped robot in both sagittal and frontal plane. The investigation shows that the swing foot of the biped robot while crossing the ditch is following the cubic polynomial trajectory. It has also been observed that all the links and joint angles make proper gait without any fail and generate dynamically balanced gaits while crossing the ditch in both sagittal and frontal planes.

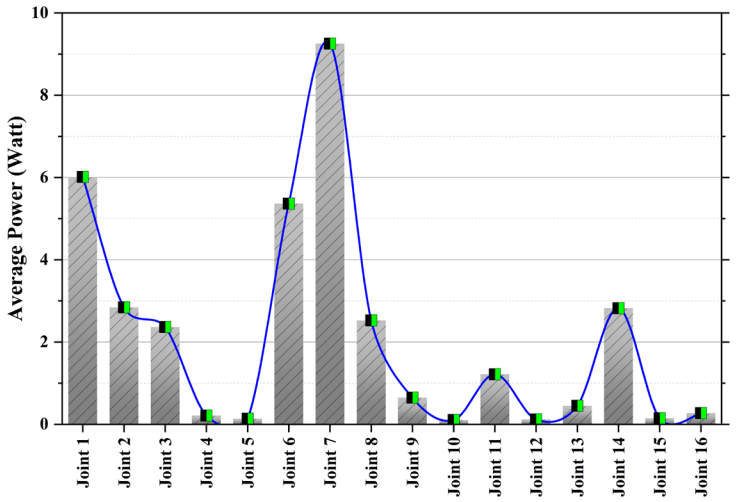

Schematic diagram showing the variation of average power consumption at different joints

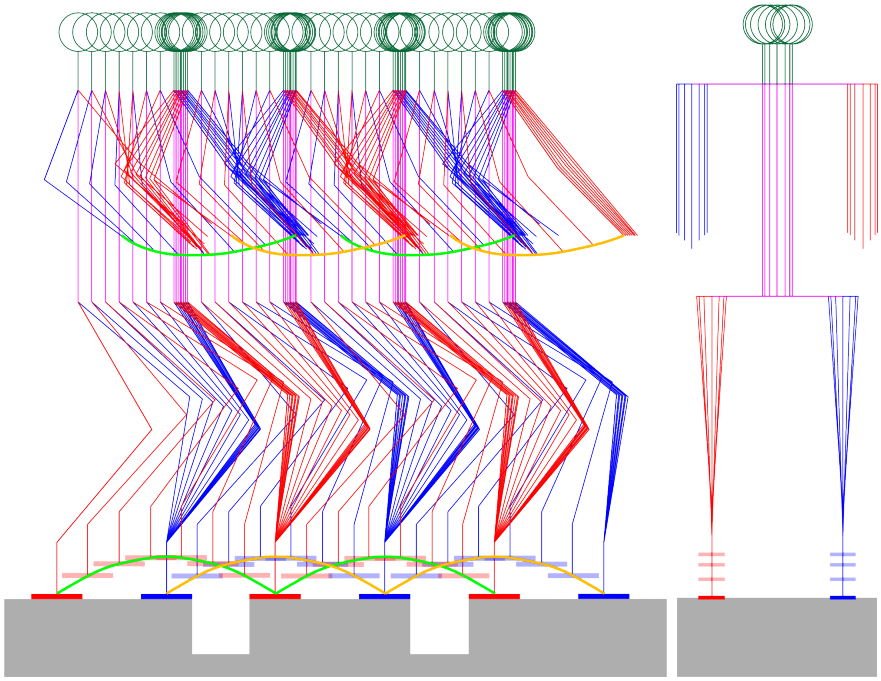

Figure 11
Stick diagram showing simulation of 16-DOF biped robot while crossing the ditch (a) sagittal plane and (b) frontal plane

Finally, the obtained gait angles from the simulations are fed into the real biped robot (that is, AZAD-16) developed in the Robotics Lab at MANIT Bhopal is shown in Figure 12. From Figure 12 it can be seen that the AZAD-16 biped robot generates a dynamically balanced gait while crossing the ditch in real time.

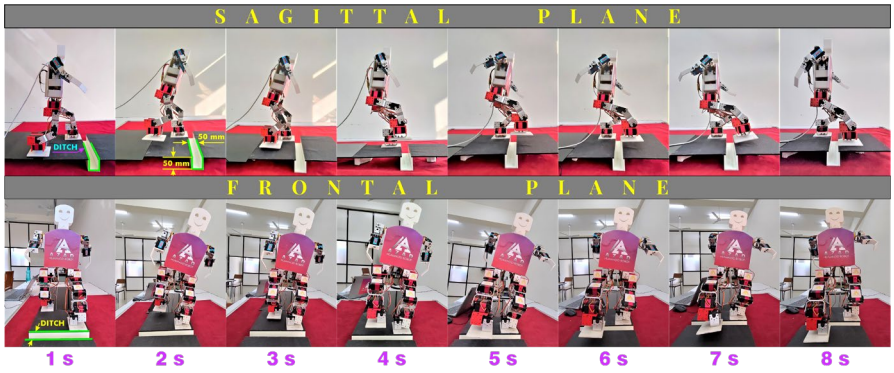

AZAD-16 performing the ditch crossing gait in the sagittal plane and frontal plane

Conclusion

In the present investigation, the authors successfully attempted to generate a gait for crossing ditch in both sagittal and frontal planes. Initially, the polynomials such as quadratic (second order), cubic (third order) and quintic (fifth order) are assigned for the swing foot while crossing the ditch. The result shows the cubic polynomial of the swing foot trajectory performing a more dynamically balanced gait when compared to quadratic and quintic polynomial trajectories. The concept of inverse kinematics has been adopted for obtaining the various joint angles. The dynamics of the 16-DOF biped robot is calculated by using the Lagrange-Euler formulation which helped in determining the torque at each joint of the biped robot. The hip joints of the swing and stance foot required more torque while crossing the ditch when compared to other joints of both the swing and stance leg. Moreover, research also reveals that the torque required at the hip joint of the swing leg is high as compared with the stance leg. Further, the knee joint of the biped robot consumes less torque than the hip joint but generates the highest torque among the rest of the other joints. A simulation study has been conducted in MATLAB. Finally, the obtained joint angles are fed into the real biped robot that is, AZAD-16 and verified the simulation study with the real biped robot walking in terms of dynamic balance margin (DBM).

References

[1] M. Vukobratovic, A. A. Frank, and D. Juricic, “On the Stability of Biped Locomotion,” *IEEE Trans. Biomed. Eng.*, vol. BME-17, no. 1, pp. 25–36, Jun. 1970, doi: 10.1109/TBME.1970.4502681.

[2] C. K. Chow and D. H. Jacobson, “Further studies of human locomotion:

Postural stability and control," *Math. Biosci.*, vol. 15, no. 1–2, pp. 93–108, Jun. 1972, doi: 10.1016/0025-5564(72)90065-X.

[3] M. A. Townsend and T. C. Tsai, "Biomechanics and modelling of bipedal climbing and descending," *J. Biomech.*, vol. 9, no. 4, pp. 227–239, Jun. 1976, doi: 10.1016/0021-9290(76)90008-7.

[4] R. Katoh and M. Mori, "Control method of biped locomotion giving asymptotic stability of trajectory," *Automatica*, vol. 20, no. 4, pp. 405–414, Jun. 1984, doi: 10.1016/0005-1098(84)90099-2.

[5] R. Katoh and M. Mori, "Control method of biped locomotion giving asymptotic stability of trajectory," *Automatica*, vol. 20, no. 1, pp. 229–234, Jun. 1982, doi: 10.1016/0005-1098(84)90099-2.

[6] T. Mita, T. Yamaguchi, T. Kashiwase, and T. Kawase, "Realization of a high speed biped using modern control theory," *Int. J. Control*, vol. 40, no. 1, pp. 107–119, Jun. 1984, doi: 10.1080/00207178408933260.

[7] Y. Hürmüzlü and G. D. Moskowitz, "The role of impact in the stability of bipedal locomotion," *Dyn. Stab. Syst.*, vol. 1, no. 3, pp. 217–234, Jun. 1986, doi: 10.1080/02681118608806015.

[8] A. Takanishi, M. Tochizawa, T. Takeya, H. Karaki, and I. Kato, "Realization of Dynamic Biped Walking Stabilized with Trunk Motion Under Known External Force," in *Advanced Robotics: 1989*, K. J. Waldron, Ed. Berlin, Heidelberg: Springer Berlin Heidelberg, 1989, pp. 299–310. [Online]. Available: http://link.springer.com/10.1007/978-3-642-83957-3_21

[9] A. Takanishi, H. Lim, M. Tsuda, and I. Kato, "Realization of dynamic biped walking stabilized by trunk motion on a sagittally uneven surface," in *IEEE International Workshop on Intelligent Robots and Systems, Towards a New Frontier of Applications*, Jun. 1990, pp. 323–330. doi: 10.1109/IROS.1990.262408.

[10] Y. F. Zheng, "A neural gait synthesizer for autonomous biped robots," in *IEEE International Workshop on Intelligent Robots and Systems, Towards a New Frontier of Applications*, Jun. 1990, pp. 601–608. doi: 10.1109/IROS.1990.262457.

[11] "Real-time neural network control of a biped walking robot," *IEEE Control Syst.*, vol. 14, no. 1, pp. 41–48, Jun. 1994, doi: 10.1109/37.257893.

[12] T. Arakawa and T. Fukuda, "Natural motion trajectory generation of biped locomotion robot using genetic algorithm through energy optimization," in *IEEE International Conference on Systems, Man and Cybernetics*, Jun. 1996, vol. 2, pp. 1495–1500. doi: 10.1109/ICSMC.1996.571368.

[13] L. Magdalena and F. Monasterio-Huelin, "A Fuzzy logic controller with learning through the evolution of its knowledge base," *Int. J. Approx. Reason.*, vol. 16, no. 3–4, pp. 335–358, Jun. 1997, doi: 10.1016/S0888-613X(97)80098-9.

[14] G. Abba and N. Chaillet, “Robot Dynamic Modeling Using a Power Flow Approach with Application to Biped Locomotion,” *Auton. Robots*, vol. 6, no. 1, pp. 39–52, Jun. 1999, doi: 10.1023/A:1008820525412.

[15] Y. Nakamura *et al.*, “Humanoid robot simulator for the METI HRP Project,” *Rob. Auton. Syst.*, vol. 37, no. 2–3, pp. 101–114, Jun. 2001, doi: 10.1016/S0921-8890(01)00152-X.

[16] J. Chestnutt, J. Kuffner, K. Nishiwaki, and S. Kagami, “Planning biped navigation strategies in complex environments,” 2003.

[17] C. Sabourin and O. Bruneau, “Robustness of the dynamic walk of a biped robot subjected to disturbing external forces by using CMAC neural networks,” *Rob. Auton. Syst.*, vol. 51, no. 2–3, pp. 81–99, Jun. 2005, doi: 10.1016/j.robot.2005.02.001.

[18] J. R. T. Puga, F. M. T. Silva, and V. M. F. Santos, “MOTION PLANNING AND CONTROL STRATEGIES FOR A DISTRIBUTED ARCHITECTURE HUMANOID ROBOT,” *IFAC Proc. Vol.*, vol. 39, no. 15, pp. 773–778, Jun. 2006, doi: 10.3182/20060906-3-IT-2910.00129.

[19] R. Ghorbani, Q. Wu, and G. G. Wang, “Nearly optimal neural network stabilization of bipedal standing using genetic algorithm,” *Eng. Appl. Artif. Intell.*, vol. 20, no. 4, pp. 473–480, Jun. 2007, doi: 10.1016/j.engappai.2006.09.007.

[20] P. R. Vundavilli and D. K. Pratihar, “Inverse dynamics learned gait planner for a two-legged robot moving on uneven terrains using neural networks,” *Int. J. Adv. Intell. Paradig.*, vol. 1, no. 1, pp. 80–109, 2008.

[21] P. R. Vundavilli and D. K. Pratihar, “Dynamically balanced optimal gaits of a ditch-crossing biped robot,” *Rob. Auton. Syst.*, vol. 58, no. 4, pp. 349–361, Jun. 2010, doi: 10.1016/j.robot.2009.10.004.

[22] P. R. Vundavilli and D. K. Pratihar, “Gait Planning of Biped Robots Using Soft Computing: An Attempt to Incorporate Intelligence BT - Intelligent Autonomous Systems: Foundations and Applications,” D. K. Pratihar and L. C. Jain, Eds. Berlin, Heidelberg: Springer Berlin Heidelberg, 2010, pp. 57–85. doi: 10.1007/978-3-642-11676-6_4.

[23] A. Fattah and A. Fakhari, “Trajectory planning of walking with different step lengths of a seven-link biped robot,” in *International Design Engineering Technical Conferences and Computers and Information in Engineering Conference*, 2010, vol. 44106, pp. 1361–1369.

[24] A. P. Sudheer, R. Vijayakumar, and K. P. Mohandas, “Optimum stable gait planning for an 8 link biped robot using simulated annealing,” *Int. J. Simul. Model.*, vol. 10, no. 4, pp. 177–190, 2011.

[25] N. Kalamian and M. Farrokhi, “Dynamic walking of biped robots with obstacles using predictive controller,” in *2011 1st International eConference on Computer and Knowledge Engineering (ICCKE)*, 2011, pp. 105–110. doi: 10.1109/ICCKE.2011.6413334.

[26] L. S. R. Lathan, B. N. S. Rani, and P. R. Vundavilli, "Analytical approach for generating dynamically balanced gaits for obstacle crossing biped robot," in *IEEE-International Conference On Advances In Engineering, Science And Management (ICAESM-2012)*, 2012, pp. 187–191.

[27] M. R. Kumar, L. S. Lathan, and P. R. Vundavilli, "Dynamically balanced obstacle crossing gait generation of a biped robot using neural networks," *Int. J. Mech. Robot. Syst.*, vol. 2, no. 3–4, pp. 232–253, 2015.

[28] R. K. Mandava and P. R. Vundavilli, "Whole body motion generation of 18-DOF biped robot on flat surface during SSP & DSP," *Int. J. Model. Identif. Control*, vol. 29, no. 3, pp. 266–277, 2018.

[29] R. K. Mandava and P. R. Vundavilli, "An analytical approach for generating balanced gaits of a biped robot on stairs and sloping surfaces," *Int. J. Model. Identif. Control*, vol. 33, no. 1, pp. 28–50, 2019.

[30] R. K. Mandava, K. Mrudul, and P. R. Vundavilli, "Dynamic motion planning algorithm for a biped robot using fast marching method hybridized with regression search," *Acta Polytech. Hung*, vol. 16, pp. 189–208, 2019.

[31] K. Bai, Y. Luo, G. Jiang, G. Jiang, and L. Guo, "High torque realization of the stepping over gait for a humanoid robot," *Ind. Robot Int. J. Robot. Res. Appl.*, vol. 47, no. 4, pp. 473–487, Jan. 2020, doi: 10.1108/IR-10-2019-0206.

[32] H. P. H. Anh and T. T. Huan, "Optimal walking gait generator for biped robot using modified Jaya optimization technique," *Int. J. Comput. Intell. Syst.*, vol. 13, no. 1, p. 382, 2020.

[33] M. Tsuru, A. Escande, A. Tanguy, K. Chappellet, and K. Harad, "Online Object Searching by a Humanoid Robot in an Unknown Environment," *IEEE Robot. Autom. Lett.*, vol. 6, no. 2, pp. 2862–2869, Jun. 2021, doi: 10.1109/LRA.2021.3061383.

[34] L. Yang, G. Lai, Y. Chen, and Z. Guo, "Online Control for Biped Robot with Incremental Learning Mechanism," *Appl. Sci.*, vol. 11, no. 18, p. 8599, 2021.

[35] A. K. Kashyap, D. Parhi, and A. Pandey, "Improved Modified Chaotic Invasive Weed Optimization Approach to Solve Multi-Target Assignment for Humanoid Robot," *J. Robot. Control*, vol. 2, no. 3, Jun. 2021, doi: 10.18196/jrc.2377.

[36] A. K. Kashyap and D. R. Parhi, "Optimization of stability of humanoid robot NAO using ant colony optimization tuned MPC controller for uneven path," *Soft Comput.*, vol. 25, no. 7, pp. 5131–5150, Jun. 2021, doi: 10.1007/s00500-020-05515-1.

[37] V. Janardhan and R. Prasanth Kumar, "Online trajectory generation for wide ditch crossing of biped robots using control constraints," *Rob. Auton. Syst.*, vol. 97, pp. 61–82, Jun. 2017, doi: 10.1016/j.robot.2017.07.014.

[38] G. Gupta and A. Dutta, "Trajectory generation and step planning of a 12 DoF biped robot on uneven surface," *Robotica*, vol. 36, no. 7, pp. 945–970, 2018